

# Laminar free convection in confined regions

By M. GRAE WORSTER†

D.A.M.T.P., Silver Street, Cambridge, CB3 9EW, England

AND ALISON M. LEITCH‡

R.S.E.S., Australian National University, G.P.O. Box 4, Canberra A.C.T. 2601, Australia

(Received 31 January 1985)

We investigate the development of density stratification in a confined fluid due to a buoyancy source which gives rise to a vertical convective boundary layer. We find that the stratification is significantly different when the boundary layer is laminar rather than turbulent. In particular, the magnitude of the density gradient in the fluid interior increases rather than decreases in the direction of flow of the boundary layer, and this density gradient varies smoothly so that there is no density front between the stratified fluid and the unmodified homogeneous fluid. Laboratory experiments are described in which homogeneous fluid in a rectangular container was heated at a vertical sidewall. Vertical temperature profiles and streak photographs were taken which show the dominant features of the stratification mechanism under laminar flow conditions. We review similarity theory for a vertical, laminar, free-convection boundary layer in a homogeneous environment, and develop new similarity solutions for convective boundary layers in stratified environments. We use these analytic results to interpret qualitative features of the experimentally observed flow fields and to develop an expression for the depth of the stratified layer as a function of time.

---

## 1. Introduction

Fluid motion driven by buoyancy supplied at a point source or at a vertical plane wall is often confined principally to a narrow boundary layer. If such free convection occurs in a confined fluid region then over time it can significantly modify the fluid outside the boundary layer. In particular, a stable density gradient can be produced in a fluid that is initially homogeneous. This phenomenon has become known as the filling-box process (Turner 1979).

The most commonly considered type of filling box is that in which a turbulent plume arises from either a point source or a line source of buoyancy. Such a system was first analysed by Baines & Turner (1969). Their model has since been applied in a wide range of practical situations including the explanation of stratification in the oceans (e.g. Killworth 1977), in tanks containing liquid natural gas (Germeles 1975) and in magma chambers (Sparks, Meyer & Sigurdsson 1980).

The success of this model and the physical ideas inherent in it have greatly influenced people's intuitive thinking about filling boxes. However, in this paper we show that the fundamentally different dynamics of a laminar convective boundary

† Current address: Massachusetts Institute of Technology, Cambridge, Massachusetts 02139, U.S.A.

‡ Current address: Erindale Campus, University of Toronto, Mississauga, Ontario, Canada L5L 1C6.

layer lead to significant qualitative differences in the stratification of the filling box. Interest in such laminar filling boxes has grown recently in the context of magma chambers. Both cooling and crystallization at the sidewalls of magma chambers lead to convection there, and this convection may be responsible for the thermal and compositional stratification of the chambers (McBirney 1980; Chen & Turner 1980; Leitch 1985). Since the Prandtl number,  $\sigma = \nu/\kappa$  where  $\nu$  is the kinematic viscosity and  $\kappa$  the thermal diffusivity, of magma is typically between  $10^2$  and  $10^4$ , we focus our attention on laminar convection in fluids of large Prandtl number.

The work presented in this paper is principally experimental, but useful physical insight is gained from an analytic study of laminar free-convection boundary layers. In §2, similarity theory for convective boundary layers in homogeneous environments is briefly reviewed, and new similarity solutions are found for convective boundary layers in a particular family of stratified environments. The results of §2 are used in §3 to develop a simple theoretical model of a laminar filling box and in §5 to aid our interpretation of the experimental observations.

Filling boxes with buoyancy supplied at the vertical sidewalls of a rectangular fluid region have been investigated by Schwind & Vliet (1964). In their experiments a constant heat flux was supplied (via electrically heated vertical plates) and the conditions were such that the boundary layers were turbulent for at least part of their ascent. In our experiments (described in §4) buoyancy was supplied via a constant-temperature sidewall and the flow was always laminar. Transition to turbulence is determined by the magnitude of the Rayleigh† number  $Ra = \alpha g \Delta T h^3 / \kappa \nu$ , where  $\alpha$  is the coefficient of thermal expansion,  $g$  is the acceleration due to gravity,  $h$  is the fluid depth and  $\Delta T$  is a characteristic temperature scale. We were careful to ensure laminar flow by having a small temperature difference between the isothermal wall and the homogeneous fluid, a shallow fluid depth, and by using a mixture of glycerine and water which had a viscosity about twice that of pure water.

Temperature profiles were obtained during the experiments to show the development of stratification in the fluid and to determine the rate of growth of the stratified layer. Streak photographs were taken of the flow field to reveal important aspects of the filling-box mechanism and the interaction between the environment and the boundary layer. In §6 the experimental observations and measurements are drawn together with the similarity solutions to form a complete picture of the filling-box process under conditions of laminar flow.

## 2. Laminar convective boundary layers

The filling boxes that we wish to consider are typified by having a laminar convective boundary layer at a vertical sidewall of a finite fluid container. A proper understanding of the dynamics of the boundary layer will aid interpretation of the observed evolution of such filling boxes. Thus, before the experiments are described, we shall examine the behaviour of laminar, free-convection boundary layers in unbounded homogeneous and stratified environments.

The boundary-layer equations for steady two-dimensional convection adjacent to a vertical plane wall are

$$uw_x + ww_z = \nu w_{xx} + \alpha g(T - T_i), \quad (1)$$

$$uT_x + wT_z = \kappa T_{xx} \quad (2)$$

† Some authors prefer to use the Grashof number  $Gr = \sigma^{-1} Ra$ . However, use of the Rayleigh number gives a more natural scaling of the boundary-layer equations when  $\sigma \gg 1$ , as will be seen in §2.

(Turner 1979), where  $u$  and  $w$  are the velocity components corresponding to the horizontal direction  $x$  and the vertical direction  $z$  respectively,  $T$  is the local temperature and  $T_1(z)$  is the horizontally uniform temperature of the ambient fluid. The Boussinesq approximation has been used in the derivation of (1) and (2) so that the physical parameters  $\nu$ ,  $\kappa$  and  $\alpha$  (defined in the Introduction) are treated as constants, and variations in density are ignored except insofar as they provide a buoyancy forcing in the momentum equation. Mass conservation is satisfied by the introduction of a stream function  $\psi$  such that

$$u = -\psi_z, \quad w = \psi_x. \tag{3}$$

It is now well known that similarity solutions to (1)–(3) exist for the special cases of a uniform environment with either an isothermal sidewall (Ostrach 1964; Turner 1979) or a sidewall with constant applied heat flux (Sparrow & Greg 1956). Here, these results are extended to cover a particular family of stratified environments. Similarity solutions can still be obtained if the temperature difference between the environment and an isothermal sidewall is proportional to any power of the height  $z$  above the leading edge. The temperature of the ambient fluid can then be written as

$$T_1 = T_w - \Delta T Ra_z^{-m}, \tag{4}$$

where  $T_w$  is the temperature of the vertical wall,  $\Delta T$  is a characteristic scale for temperature variations, and  $Ra_z$  is a local Rayleigh number defined by

$$Ra_z = \frac{\alpha g \Delta T z^3}{\kappa \nu}. \tag{5}$$

The temperature difference between wall and environment is thus proportional to  $z^{-3m}$ , and the environment is stably stratified if  $m > 0$ . The stream function and the temperature perturbation can now be written in terms of the similarity variable

$$\xi = Ra_z^{\frac{1}{2}(1-m)} \frac{x}{z}, \tag{6}$$

as

$$\psi = \kappa Ra_z^{\frac{1}{2}(1-m)} \bar{F}(\xi), \tag{7}$$

and

$$T - T_1(z) = \Delta T Ra_z^{-m} G(\xi). \tag{8}$$

The non-dimensional functions  $F$  and  $G$  satisfy the ordinary differential equations

$$F''' + \frac{1}{\sigma} \left[ \frac{3}{4}(1-m) FF'' - \frac{1}{2}(1-3m) F'^2 \right] + G = 0, \tag{9}$$

$$G'' + \frac{3}{4}(1-m) FG' - 3m(1-G)F' = 0, \tag{10}$$

subject to the boundary conditions

$$F = F' = 0, \quad G = 1 \quad (\xi = 0), \tag{11}$$

$$F' \rightarrow 0, \quad G \rightarrow 0 \quad (\xi \rightarrow \infty). \tag{12}$$

Equations pertaining to a homogeneous environment, which were investigated by Ostrach (1964), are obtained by setting  $m = 0$  in (9)–(12). Ostrach integrated the equations numerically for various values of the Prandtl number. Two solutions are illustrated in figure 1; one for  $\sigma = 1$ , the other for  $\sigma = 16$ , which is the Prandtl number of our experimental fluid. The main feature of interest to us here is that the lateral scales of the thermal and viscous boundary layers become widely separated as  $\sigma$  increases. In the next section a simple model of a laminar filling box will be developed

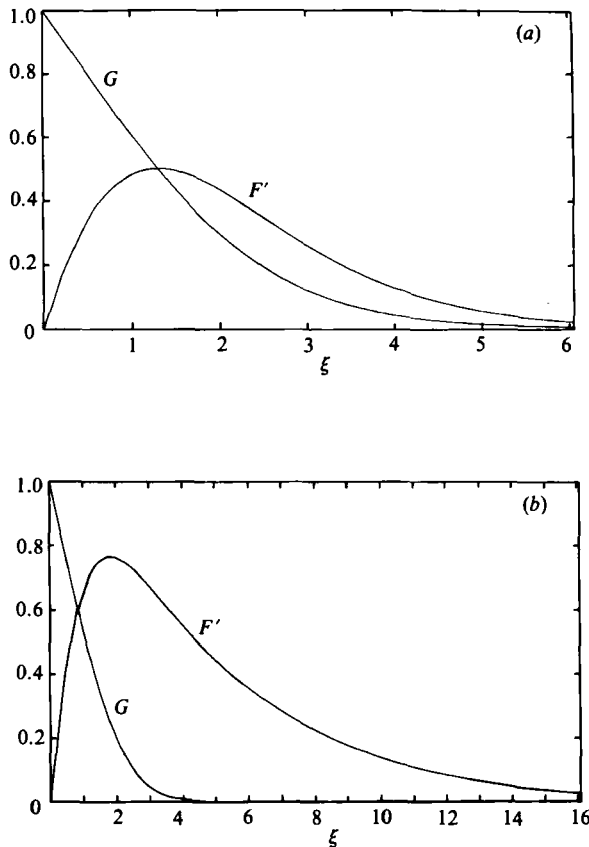


FIGURE 1. Similarity solutions for a laminar wall layer in a homogeneous environment: the temperature profile  $G$  and the vertical velocity profile  $F'$ . (a) Prandtl number  $\sigma = 1$  and (b)  $\sigma = 16$ .

based on the assumption that the growth rate of the stratified region is determined solely by the mass flux of the inner, thermal boundary layer.

Laminar flow is most likely to occur when the fluid viscosity and, hence, the Prandtl number are large. Numerical integration of the governing equations becomes increasingly difficult as  $\sigma$  increases so it is useful to perform an asymptotic analysis which is formally valid in the limit  $\sigma \rightarrow \infty$ . This has the added bonus that the dependence of the solutions on  $\sigma$  is made explicit so that the analytic results, supported by our experiments at  $\sigma = 16$ , may be easily extrapolated for situations where  $\sigma$  is large and different from 16. Kuiken (1968) showed that the asymptotic theory is reasonable for  $\sigma \gtrsim 2$  and is in good agreement with the finite-Prandtl-number results for  $\sigma \gtrsim 10$ .

Kuiken obtained the equations governing the leading-order behaviour of the inner layer by letting  $\sigma \rightarrow \infty$  in (9) and (10) (with  $m = 0$ ) to give

$$F''' + G = 0, \quad (13)$$

and

$$G'' + \frac{3}{4}FG' = 0, \quad (14)$$

subject to the boundary conditions (11) and matching conditions with an outer solution which require

$$F'' \rightarrow 0, \quad G \rightarrow 0 \quad (\eta \rightarrow \infty). \quad (15)$$

We have integrated these equations numerically and present a graph of  $F$  as a

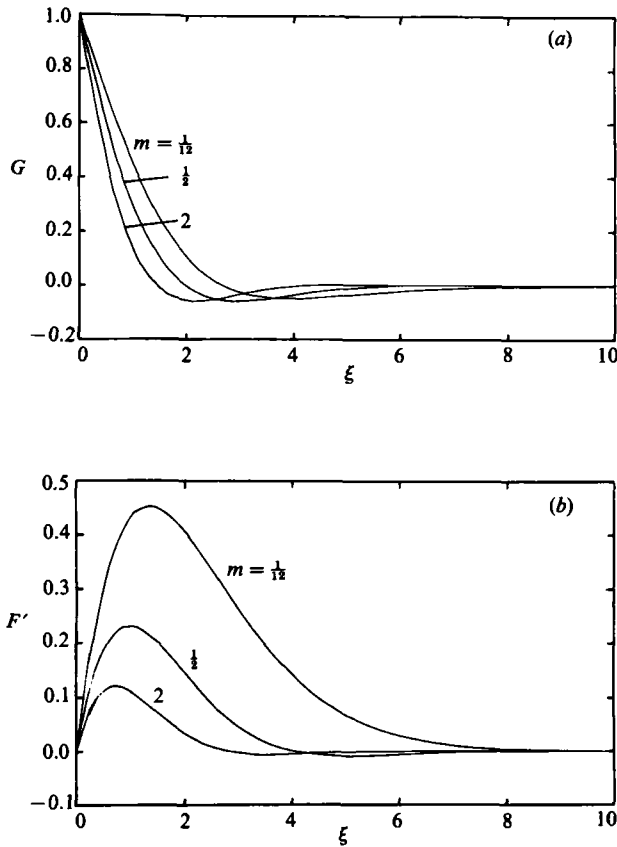


FIGURE 2. Similarity solutions for laminar wall layers in various stratified environments at infinite Prandtl number. The density gradient in the environment increases as  $m$  increases (see (4)).

function of  $G$  in figure 9. The dashed curve in figure 9 represents  $F(G)$  evaluated for  $\sigma = 16$  and is included for comparison with the result at infinite Prandtl number. The function  $F(G)$  in the inner layer is needed in the next section to determine the rate of stratification in a filling box.

Finally in this section, we examine the effect of stratification upon the boundary layer. Gill (1966) considered the asymptotic behaviour at the outer edge of a boundary layer in a stably stratified fluid and thereby showed first that the lateral scales of the thermal and viscous layers have the same order of magnitude in the limit  $\sigma \rightarrow \infty$ , and secondly that the boundary layer may either entrain or detraining. These features, fundamental to our understanding of the laminar filling box, are illustrated by the family of solutions specified by (6)–(12).

From (7) we see that the boundary layer represented by the similarity solution is entraining ( $\psi$  increases with  $z$ ) for  $0 \leq m < 1$  and is detraining ( $\psi$  decreases with  $z$ ) for  $m > 1$ . Since the thermal and viscous layers have the same order of magnitude in a stratified environment we can apply the boundary conditions (12) together with (11) to the equations governing the large-Prandtl-number behaviour (10) and (13). These solutions are displayed in figure 2. The curves for  $m = \frac{1}{12}$  and  $m = \frac{1}{2}$  correspond to entraining boundary layers while the curve for  $m = 2$  corresponds to a detraining layer.

Note first that there is a small negative temperature perturbation in the outer part

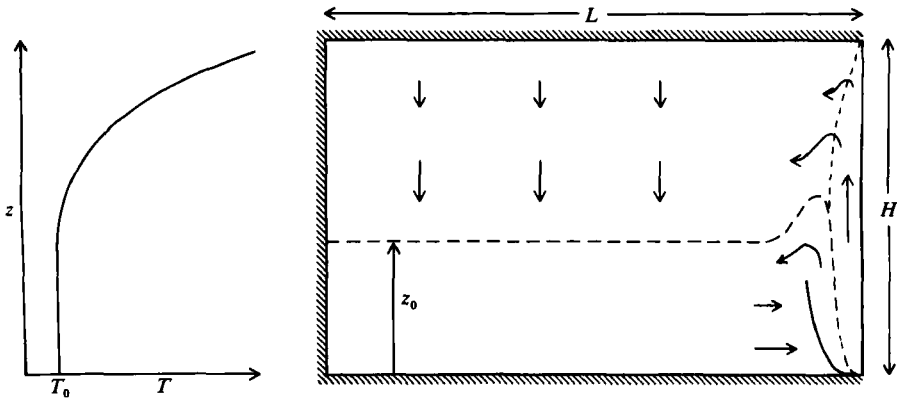


FIGURE 3. The stratification in the environment and the fluid motions in a filling box with a laminar wall layer. The boundary layer has a two-layer structure where the environment is homogeneous. The outer boundary layer detrains just below  $z = z_0$ , and a narrower boundary layer remains, with only one-layer structure, where the environment is stratified.

of the layers. This is due to fluid from the stratified environment being dragged upwards, by viscous contact with the inner boundary layer, above its equilibrium density level. If the stratification of the environment is sufficiently steep then this negative temperature perturbation can force a downflow in the outer part of the boundary layer. This is demonstrated by the solutions for  $m = \frac{1}{2}$  and  $m = 2$ . We can now understand physically why the lateral scale of the viscous boundary layer is restricted to the same order of magnitude as the thermal layer when the environment is stably stratified. When the environment is homogeneous, viscous stresses at the edge of the buoyant layer need only do work against viscous dissipation in order to lift the outer fluid. The velocity boundary layer thus has a width characteristic of the viscous-diffusion lengthscale. When the environment is stably stratified the viscous stresses have to supply potential energy in order to raise outer fluid through the stratification. Since much more work is required per unit volume of raised fluid, less of the environment can be dragged upwards.

### 3. A simple filling-box model

The qualitative ideas and some of the numerical results of the previous section can be used to develop a simple model of a filling box having a laminar sidewall boundary layer. Suppose that the base of the stratified region is well defined and at a height  $z_0$  above the tank bottom (figure 3). The boundary layer below  $z = z_0$  may be represented by the similarity solution (6)–(12) with  $m = 0$ . It will have the double structure and large mass flux characteristic of a convective boundary layer in a homogeneous environment. For  $z > z_0$  the boundary layer will have the single-layer structure and reduced mass flux associated with convective layers in stably stratified environments. We therefore assume that all the fluid from the outer viscous layer flows out into the environment below the stratified region. Now it is readily shown, by appropriate scaling of the full Navier–Stokes and thermal-energy equation, that the temperature and vertical velocity in the environment are horizontally uniform (Gill 1966). Therefore, by mass conservation, the rate of growth of the stratified layer is given by

$$-L \frac{dz_0}{dt} = \psi_0(z_0), \quad (16)$$

where  $L$  is the length of the tank and  $\psi_0$  is the net vertical mass flux in the inner thermal layer at  $z = z_0$ . The similarity solution (6)–(8), (13)–(15) is now used to express (16) as

$$-L \frac{dz_0}{dt} = \kappa Ra_H^{\frac{1}{4}} \left( \frac{z_0}{H} \right)^{\frac{3}{4}} F(G_\infty), \quad (17)$$

where  $H$  is the height of the tank and  $Ra_H$  is the Rayleigh number based on  $H$ . The mass flux of the inner layer is determined only in terms of some non-dimensional temperature  $G_\infty$  chosen to define the edge of the layer and also the base of the stratified region. Equation (17) is readily integrated to yield

$$\frac{z_0}{H} = \left( 1 - \frac{1}{4} Ra_H^{\frac{1}{4}} F(G_\infty) \frac{\kappa}{LH} t \right)^{\frac{4}{3}}, \quad (18)$$

or, in non-dimensional variables, as

$$\zeta_0 = (1 - F(G_\infty) \tau)^{\frac{4}{3}}, \quad (19)$$

where  $\zeta_0 = z_0/H$  and  $\tau = \frac{1}{4} Ra_H^{\frac{1}{4}} (\kappa/LH) t$ . This expression, giving the depth of the stratified layer as a function of time, is one of the central results of the present paper. It can be compared with the rather different forms of the stratification depth in a filling box driving by an axisymmetric turbulent plume,

$$\zeta_0 = (1 + \frac{1}{5} (\frac{18}{5})^{\frac{1}{2}} \tau_1)^{-\frac{2}{3}}, \quad (20)$$

or by turbulent line plume

$$\zeta_0 = e^{-\tau_2}, \quad (21)$$

where  $\tau_1$  and  $\tau_2$  are suitably non-dimensionalized times (Baines & Turner 1969; Worster & Huppert 1983). In all cases the stratification rate decreases with time; but for the turbulent plumes the tank is never stratified to the base, whereas it is clear from (19) that the laminar layer stratifies the whole tank in a time

$$t_0 = 4 Ra_H^{-\frac{1}{4}} [F(G_\infty)]^{-1} \frac{LH}{\kappa}, \quad (22)$$

which is faster than the characteristic diffusion time by a factor of order  $Ra_H^{\frac{1}{4}}$ . It is interesting to note that Patterson & Imberger (1980), using scaling arguments, obtained a similar stratification timescale for a system differentially heated and cooled from opposite, isothermal sidewalls. They found  $t_0 \propto Ra^{-\frac{1}{4}} LH/\kappa$ . The values of the multiplying constant  $4[F(G_\infty)]^{-1}$ , as determined both from the similarity solutions and from our experimental observations, are displayed in figure 9.

The model presented in this section is an oversimplified account of the filling-box process. Its limitations will be discussed when its conclusions are compared with the experimental results in §5.

#### 4. Experimental apparatus and procedure

The experiments were performed in a glass tank 20 cm wide filled to a depth of 20 cm with a mixture of glycerine (30 wt %) and water (see figure 4). The length of the tank was varied so that results were obtained for aspect ratios (length:height) of 1, 2 and 3. Glycerine was used to increase the viscosity of the fluid to ensure laminar flow and so that the experiments would be appropriate to the large-Prandtl-number theory. A more concentrated solution could not be used without introducing an undesirably large temperature dependence to the viscosity. The mixture had a

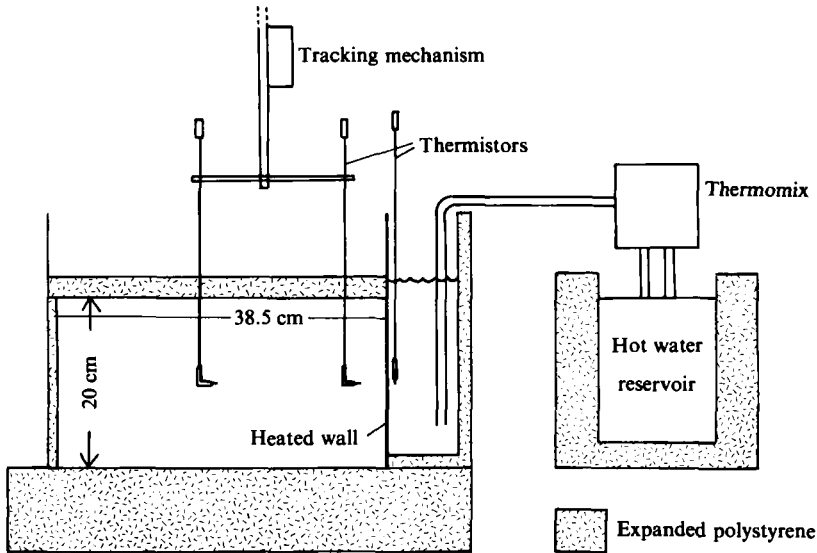


FIGURE 4. The apparatus used for the heated-sidewall experiments.

kinematic viscosity of  $(2.0 \pm 0.3) \times 10^{-2} \text{ cm}^2 \text{ s}^{-1}$  over the temperature range (22–30 °C) used in the experiments. The viscosity was measured from small samples taken just after the end of each experiment while values of other parameters, such as the thermal diffusivity ( $\kappa \approx 1.2 \times 10^{-3} \text{ cm}^2 \text{ s}^{-1}$ ) and expansion coefficient ( $\alpha \approx 3.8 \times 10^{-4} \text{ }^\circ\text{C}^{-1}$ ), were taken from a list of tables (Segur 1953). These parameter values give a Rayleigh number of about  $6 \times 10^8$ . The critical Rayleigh number for significant departure from laminar flow has been found experimentally using water ( $\sigma \approx 7$ ) to be approximately  $10^{10}$  (Elder 1965) and it increases in proportion to  $\sigma^2$  (Hieber & Gebhart 1971). Thus the experiments were performed well within the laminar-flow regime. The fluid was deaerated under vacuum to prevent bubbles from forming which could have disrupted the boundary layer on the heated wall.

A constant-temperature sidewall was produced by inserting a reservoir, made of  $\frac{1}{16}$  in. copper sheet and filled with warm water, into one end of the glass tank. All sides of the reservoir other than that exposed to the experimental fluid were insulated. The water in the reservoir was heated and recirculated with the water in a 10 l bath (at a rate of 0.2 l/s) by a Braun 1480 Thermomix. The temperature of the heated wall was measured by a thermistor and logged on a PDP11 computer which controlled the heating element of the Thermomix. In this way the temperature in the reservoir could be maintained to within  $\pm 0.03$  °C of the desired wall temperature, except in the first few minutes of the experiment when the initial very rapid heat transfer to the experimental fluid could not be matched by the turnover of hot water in the reservoir. The tank was insulated on the sides and bottom with 10 cm thick expanded polystyrene, and a sheet of 2 cm thick expanded polystyrene floated on top of the fluid. The solution was never more than a few degrees different from room temperature so there were no significant heat losses to the environment.

Temperature profiles were recorded by two thermistors; one placed near the centre of the tank, the other closer to the heated wall. These were tracked vertically through the solution by a stepper motor. Typically the thermistors were tracked at a speed of 1 mm/s, and readings were taken every two seconds. The thermistors were Fenwell fast-response glass probes (GB38P12), having a bead diameter of 0.07 in. and a



response time in air of 5 s. They were mounted at right angles to thin vertical supporting shafts so that measurements were not influenced by the wake of the shafts. The temperatures and the positions of the thermistors were logged on the computer. The accuracy of the measurements was limited by the resolution of the analog-digital converter to  $\pm 0.01$  °C for the temperatures, and to  $\pm 0.1$  mm for the positions.

Because the fluid temperature in the neighbourhood of the thermistors changed quite rapidly as they were moved through the temperature gradient, the measured temperature lagged behind the actual temperature. This was taken into account by calculating the actual temperature as

$$T = T_m + t_c \frac{dT_m}{dt}, \quad (23)$$

where  $T_m$  is the measured temperature and  $t_c$  is a characteristic response time in glycerine which is a function of the tracking speed. The value of  $t_c$  was chosen to make the temperature measurements taken while tracking upwards agree with those taken while tracking downwards. It was found that a value of  $t_c \simeq 4$  s was appropriate. This method of correcting the profile is a standard technique in oceanographical fieldwork (Horne & Toole 1980).

The flow was visualized by adding aluminium powder to the fluid and illuminating the suspension with light from a projector through a 1 cm slit opposite the heated wall. Photographs with time exposures of 8–16 s were taken periodically at right angles to the light beam. There was always some settling of the aluminium powder before an experiment began, and thus some details of the flow near the top of the tank during the very initial stages were lost. However, the settling velocities of the flakes were much slower than the convective motions, and too slow to produce streaks on the photographs.

A typical experiment would proceed as follows. The solution was deaerated, siphoned carefully into the tank and left for several hours to come into thermal equilibrium with the laboratory. Aluminium powder was added and the suspension stirred to disperse the flakes and to remove any lingering temperature variations. We waited several minutes to allow the stirring motions to die away; then a preliminary temperature profile was recorded. The copper reservoir was quickly filled with water, which was approximately 5 °C warmer than the solution, and the thermomix pump was turned on. For the first hour the thermistors were tracked up and down continuously, and photographs were taken periodically. Thereafter profiles were recorded and photographs taken every half an hour. The experiments ran for between four and six hours.

## 5. Experimental results

In this section we describe the results of the laboratory experiments and compare them with the analytical model developed in §3. In the following discussion, temperature profiles (figure 5) and streak photographs (figure 6) taken at various stages of the experiment are used to illustrate its evolution. Figure 7(*a-c*) are schematic diagrams showing the streamline patterns in figure 6(*a-c*). It is important to realize that, in a non-steady situation, the streamlines are not particle paths but are lines which are everywhere parallel to the instantaneous velocity field. The stippled areas on the diagrams represent estimates of which parts of the fluid are warm relative to the initial fluid temperature. Streamline patterns are shown only for one experiment in which the aspect ratio of the tank was 2. However, the major flow

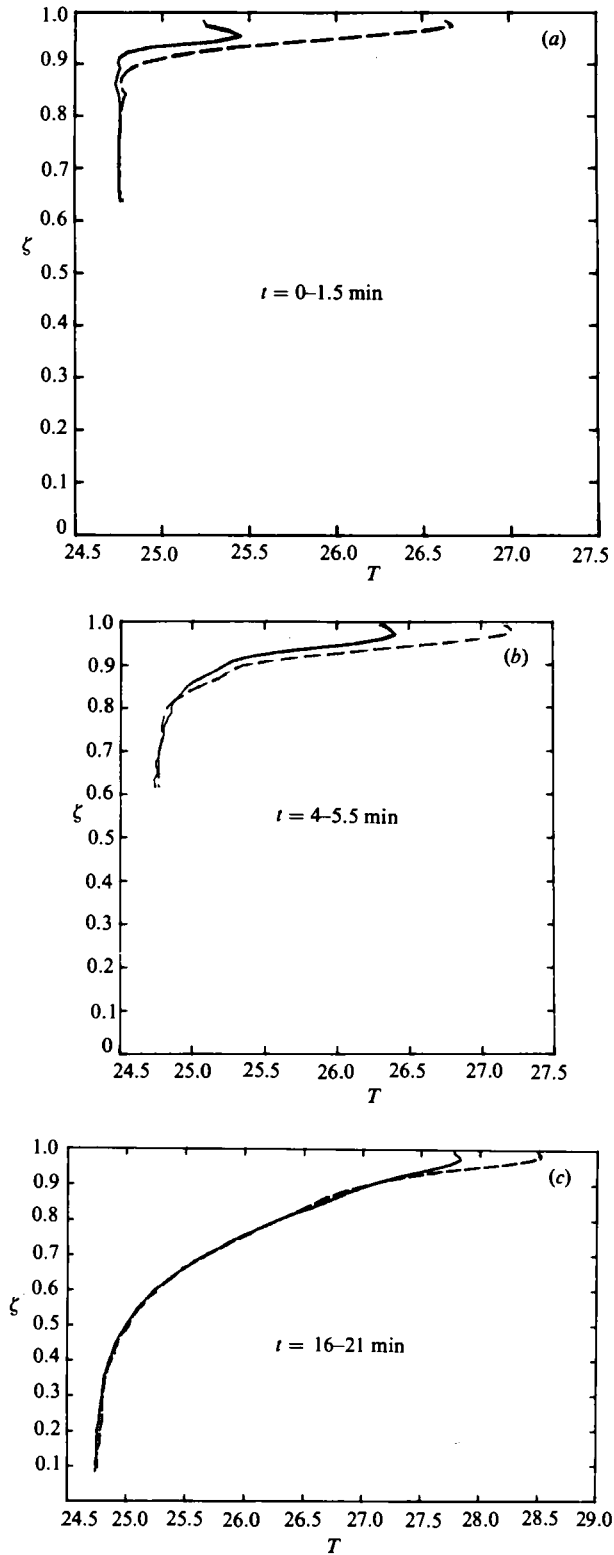


FIGURE 5 (a-c). For caption see opposite page.

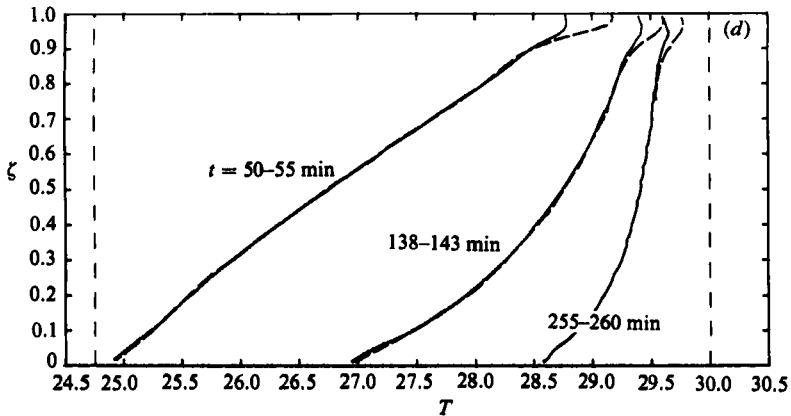


FIGURE 5. Vertical temperature profiles in the laminar filling box measured at various times  $t$  during an experiment in which the tank had an aspect ratio of 2. The dashed profiles are from the thermistor nearest the heated wall.

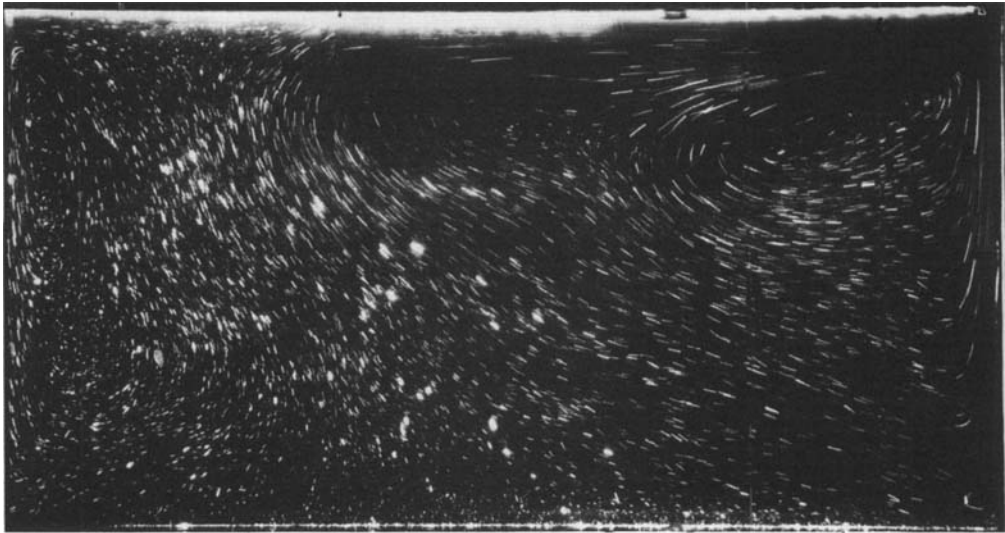
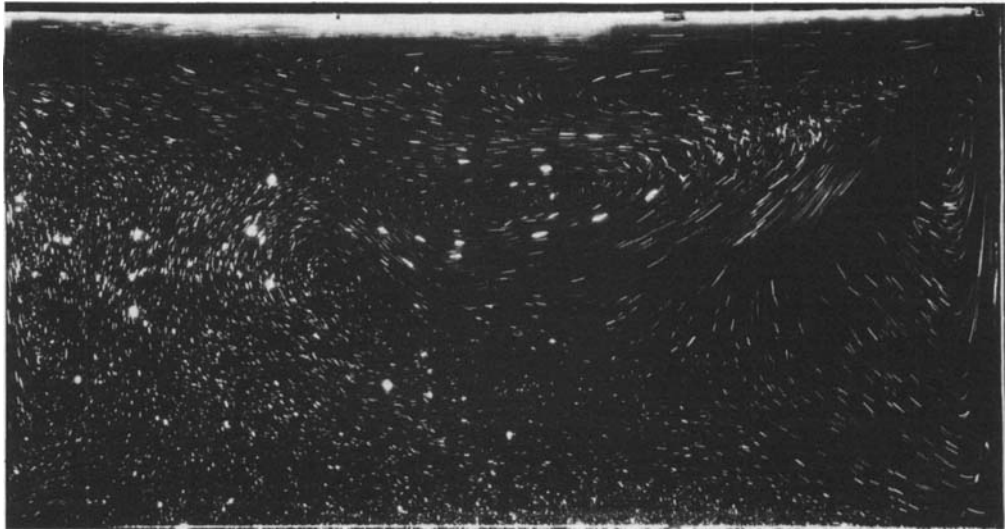
features that are to be described were similar in the other experiments where the aspect ratios were 1 and 3.

Figures 5(a), 6(a) and 7(a) show the initial development of the flow. The hot fluid from the inner thermal boundary layer flows out horizontally along the top of the tank in the form of a laminar gravity current, while fluid from the cold outer viscous boundary layer flows out underneath the warmed fluid and, unconstrained by buoyancy effects, actually recirculates back into the boundary layer in a fairly tight eddy. The profile, ignoring the inversion at the very top, which is due to the viscous drag of undisplaced cold fluid along the roof, shows the temperature gradient decreasing with distance from the top surface. The dashed profile is from the thermistor closest to the heated wall.

Other features in the flow field include a separation bubble at the top of the boundary layer, and a weak circulation at the far side of the tank. The separation bubble is believed to be an inertial effect due to the boundary-layer fluid rebounding from the roof of the tank. The weak circulation is thermal convection driven by heat from the projector lamp. This flow is soon overwhelmed by the much stronger circulation driven by the constant-temperature wall.

Figures 5(b), 6(b) and 7(b) were taken at slightly later times in the experiment. Here there is a clear separation of the detrainng boundary fluid into the warmer part, which flows horizontally along the top of the tank, and the cooler part which is forced sharply downwards by the presence of the stratified region. The stratified layer now extends right across the tank, and there is a return flow at the base of the layer where the warm outflow has reached the far end of the tank and turned around. This return flow is almost horizontal since the fluid is lighter than that below it. The outflow and return at the top is a feature which persists throughout the subsequent evolution of the system.

It is noticeable from the photographs that fluid from the cold outer viscous layer rises above its level of equal density in the stratified environment carried on by its momentum. Finding itself denser than its environment, it then flows downwards before flowing out beneath the stratified layer. The resulting negative temperature perturbation and subsequent downflow are similar to those predicted by the similarity solutions and depicted in figure 2. The downflow in the experiments is, however, much stronger than that predicted by the similarity theory. This is because

(a)  $t = 1.5$  min(b)  $t = 5$  minFIGURE 6 (*a-b*). For caption see opposite page.

the cold outer fluid gains more momentum while rising through the unstratified region than it could if the environment were stratified all the way, as it is in the similarity theory.

Strong downflow in the outer parts of the boundary layer is also apparent in figure 6(*c*), which was taken, as shown by the profile 5(*c*) and the schematic 7(*c*), when the stratification extends just over half way down the tank.

An important difference in the behaviour of a filling box fed by a laminar sidewall boundary layer rather than by a turbulent plume, is that the environment becomes stratified to the base in a finite time, as shown in §3. Once the stratification reaches the bottom of the fluid container, the nature of the laminar boundary layer changes significantly. This is demonstrated by the similarity solutions analysed in §2. There is no longer a thick outer viscous layer and therefore the downflow at the outer edge

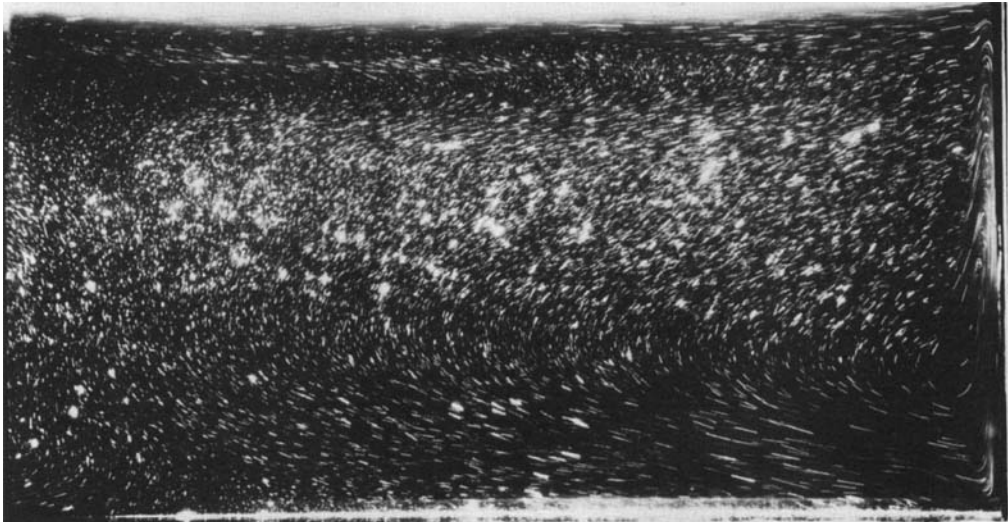
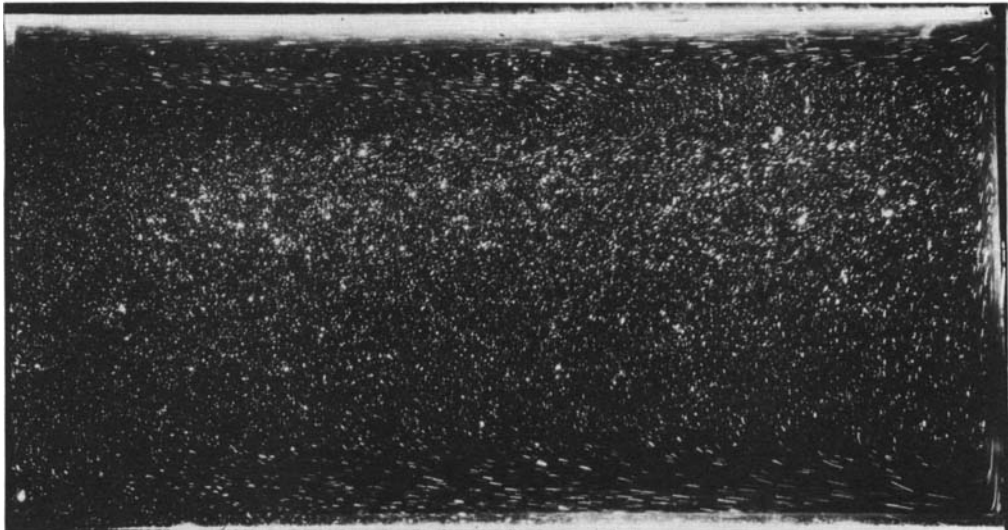
(c)  $t = 19.5$  min(d)  $t = 51.5$  min

FIGURE 6. Streak photographs of the flow field at several different times  $t$  during an experiment in which the tank had aspect ratio 2. Suspended aluminium powder is illuminated through a slit of width 1 cm in the left-hand side of the tank. (a) and (b) had 8 s exposure; (c) and (d) had 16 s exposure.

of the boundary layer is much weaker. Both these features can be seen in figure 6(d), which should be compared with figure 6(c). Entrainment increases towards the base of the boundary layer and this causes the density gradient at the bottom of the tank to lose its initial curvature and eventually to reverse it as fluid is removed from between density surfaces (see figure 5d). The final density profile, which changes quantitatively but not qualitatively as time increases further, is one in which the density gradient decreases with height near the bottom of the fluid container but increases with height near the top of the container. This S-shaped profile flattens with

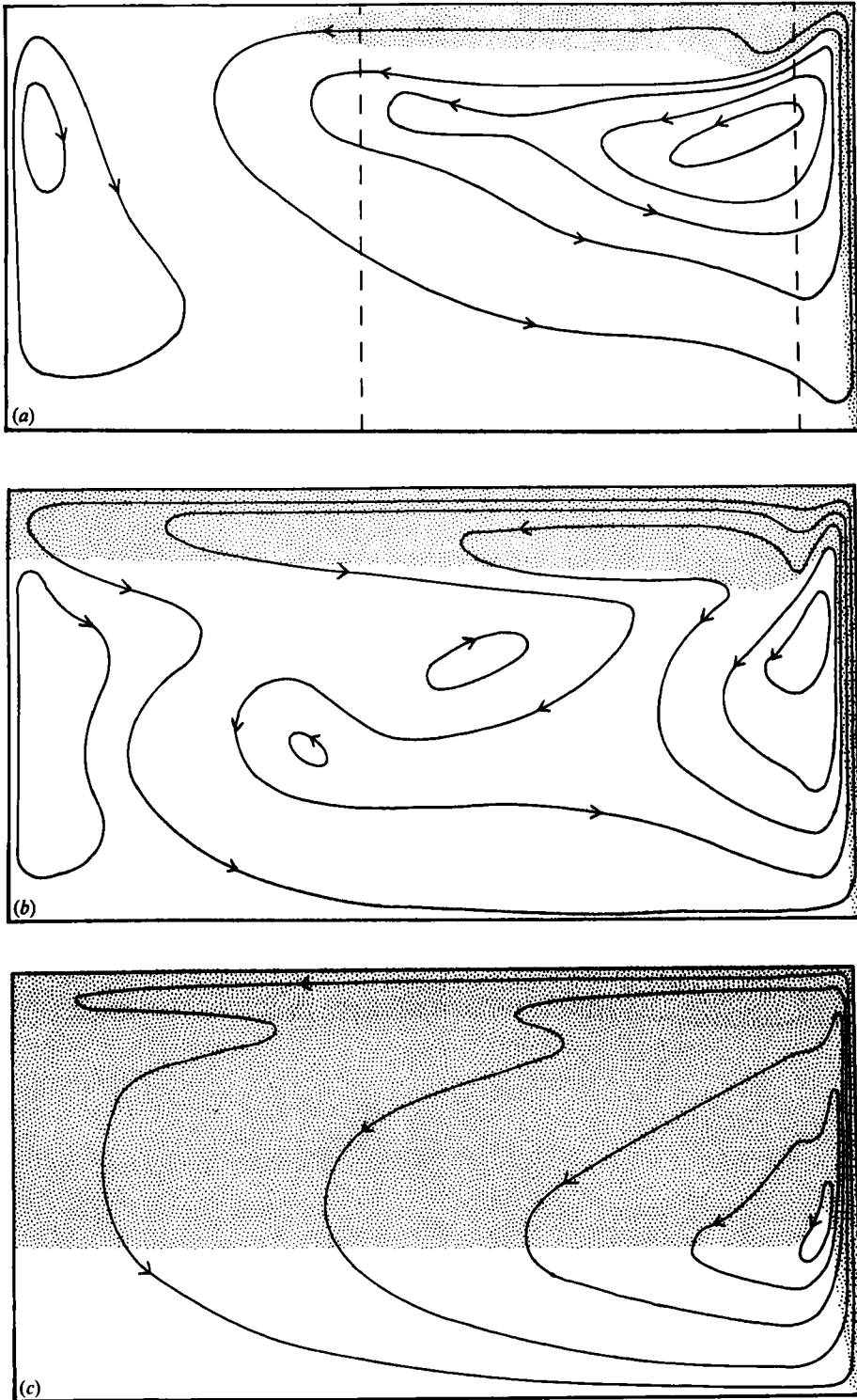


FIGURE 7. Streamline patterns traced out from the streak photographs 6(a-c). The stippling indicates where the fluid is warm relative to the initial fluid temperature. Dashed vertical lines in (a) indicate the paths of the thermistors.

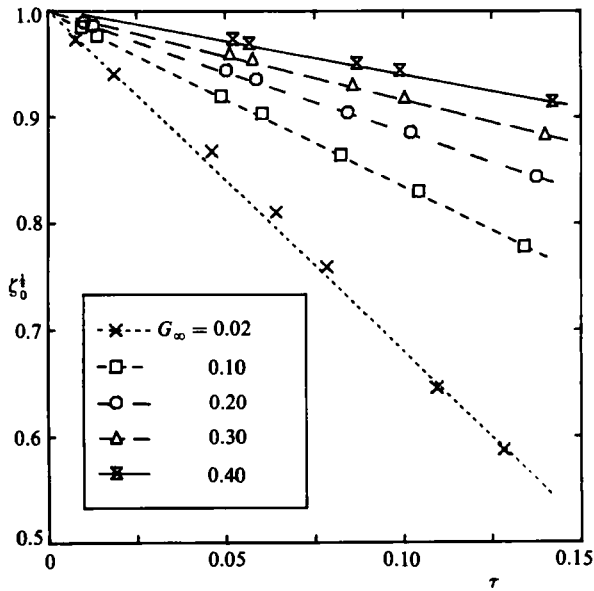


FIGURE 8. The experimentally determined position  $\zeta$  of various isotherms (of temperature  $G_\infty$ ) as a function of time  $\tau$ . The variables  $\zeta$ ,  $G_\infty$  and  $\tau$  are non-dimensional. Aspect ratio = 1.

time, as all the fluid in the tank approaches the temperature of the heated wall, and the point of inflexion moves upwards. The flow field during the later stages is typified by strong entrainment at the base of the tank, a bidirectional boundary layer, strong detrainment near the top of the tank, and a slow recirculation through the rest of the fluid. These general features, including the S-shaped density profile, are predicted by Worster (1983) for the large-time asymptotic state in a laminar filling box heated by a constant flux through a sidewall.

We now compare the quantitative results of the experiments with the theory given in §3. Equation (19), giving the height  $\zeta_0$  of the base of the stratification as a function of time  $\tau$ , was tested for several values of  $G_\infty$ , the normalized temperature defining the outer edge of the thermal boundary layer. Time was measured up to the point when the box was stratified to the base, when the density profile was approximately linear. It was found that the functional form of (19) was maintained reasonably well up to quite large values of  $G_\infty$  – that is, plots of height to the one-quarter power against time gave approximately straight lines (see figure 8). This was particularly true for the lowest-aspect-ratio experiments. There is, however, a tendency for the slopes of these lines to steepen as time increases. This is due to two effects. First, the theory assumes that the fluid below  $\zeta_0$  is unstratified: since most of the fluid in the boundary layer is entrained from near the bottom of the tank, it is as the stratification approaches the bottom that the inaccuracy of this assumption becomes noticeable. We would indeed expect the curves in figure 8 to steepen as warmer fluid is entrained into the boundary layer from below  $\zeta_0$ . Secondly, at lower depths the overshooting of boundary-layer fluid past its level of equal density in the environment is more important (figure 6*c, d*) – the mass flux of warmed fluid is then increased because the fluid remains in the boundary layer longer, absorbing more heat from the wall.

The slopes of the lines in figure 8 give values for the function  $F(G_\infty)$ . In figure 9 values of  $F(G_\infty)$  obtained from each of the experiments for five values of  $G_\infty$  are

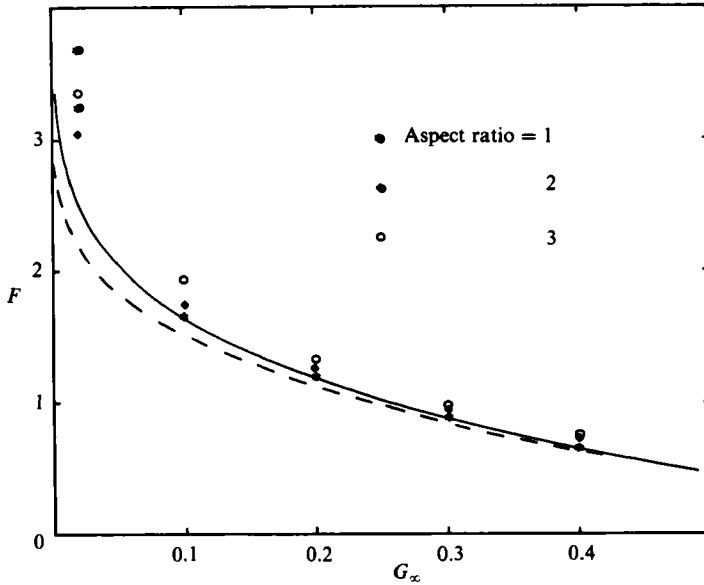


FIGURE 9. The non-dimensional volume flux  $F$  in the inner boundary as a function of the non-dimensional temperature  $G_\infty$  defining the edge of the layer. The lines are theoretical predictions of  $F$  versus  $G$ . The solid line is the infinite-Prandtl-number solution, and the dashed line is for  $\sigma = 16$ , the Prandtl number of the experiment. Superimposed are points representing the slopes of the curves of  $\zeta_0^1$  vs  $\tau$  obtained from the experimental results such as those presented in figure 8.

plotted, together with theoretical curves of  $F$  versus  $G$  predicted from the similarity solutions given in §3. Note that, except for very small values of  $G_\infty$ , there is little difference between the curve for infinite Prandtl number and that for  $\sigma = 16$ . The experimental values all lie above the theoretical curves; the agreement with theory becoming worse as the aspect ratio increases, and as  $G_\infty$  decreases below about 0.2.

The worsening agreement with increasing aspect ratio can be explained by the effects of diffusion in the environment, which the theory ignores. The value of  $F$  is obtained from the rate at which an isotherm descends in the tank, and the descent rate of an isotherm due to diffusion is given by

$$\zeta_\tau = 4 Ra^{-1} \frac{L}{H} \frac{G_\infty}{G_\zeta}. \quad (24)$$

This turns out to be about 5% of the descent rate due to the filling-box process when the aspect ratio is 2 and  $G = 0.3$ , and increases as  $G$  increases or decreases. We see that, at constant Rayleigh number, the importance of diffusion is proportional to the aspect ratio. Diffusion, then, can account for the disagreement with theory between  $G_\infty$  values of 0.1 and 0.4, but is insufficient to explain the large discrepancy at  $G_\infty = 0.02$ .

Since the non-dimensional temperature  $G_\infty$  marks the outer edge of the inner, thermal layer we might expect to get the best agreement with the theory by choosing a very small value for it. However, we see from figure 9 that the measured volume flux  $F$  is higher than that given by the theory especially for small values of  $G$ . This is because of the inertial overshooting of the boundary layer which allows the fluid to remain in contact with the hot wall for longer. Thus a larger volume flux of hot fluid is produced than is predicted by the theory. This effect is more marked the smaller the value chosen for  $G_\infty$ .



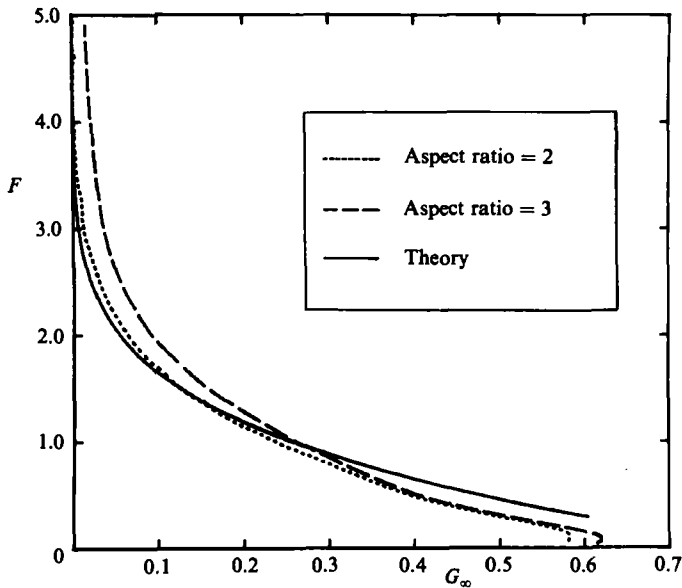


FIGURE 10. Comparison of the measured temperature profiles with the similarity theory at an early time ( $\tau = 0.05$ ) in tanks of aspect ratio 2 and 3. The profile in the tank of unit aspect ratio (not shown) is very close to that for aspect ratio 2.

Finally, in figure 10, we have plotted graphs of

$$\frac{1 - \xi^4}{\tau} \text{ versus } G, \quad (25)$$

for two sets of experimental results at some fixed small time  $\tau$ . From (18) and the definition of  $G$ , these plots should lie on the theoretical curve of  $F$  versus  $G$  as determined by the similarity theory. We see that the agreement is reasonable and improves with decreasing aspect ratio when the effects of diffusion are less important. This means that the similarity solution  $F$  versus  $G$  provides a good initial condition in the environment for possible numerical models which could follow the evolution of the system, taking into account the stratification of the environment and diffusion.

## 6. Discussion and conclusion

Experiments have been described which follow the complete time evolution of a filling box driven by a laminar sidewall boundary layer. The stratification which develops was found to be qualitatively different to that which arises in the classical case of a filling box with a turbulent plume.

The fundamental differences in the form of the stratification occur for two reasons: the horizontal outflow from the rising boundary layer is mixed in the turbulent case but unmixed in the laminar case; and the laminar boundary layer may detrain into the stratified interior, while the active engulfing of ambient fluid by large-scale eddies means that a turbulent plume always entrains until it reaches the roof. The way in which these physical differences affect the resulting stratification can now be explained by considering the small-time and large-time behaviour of the two types of filling box.

When a turbulent plume first reaches the top of the fluid container it spreads

horizontally as a well-mixed gravity current. The outflowing fluid was diluted by entrainment of ambient fluid during its rise from the source but it is still substantially lighter than the fluid below it. There is thus a large density contrast between the unmodified homogeneous fluid and the layer of buoyant fluid forming above it which Baines & Turner (1969) termed the 'first front'. Subsequent arrivals of plume fluid at the top of the container will have been diluted to almost the same extent as the first outflow but will be slightly lighter due to entrainment from the upper buoyant layer. Thus a stably stratified region grows from the top of the container with the density gradient decreasing in magnitude with height.

By contrast, when the flow is laminar the initial outflow is not mixed; individual stream surfaces retain their identity. Thus the horizontal density profile in the rising boundary layer, which increases smoothly away from the sidewall, is carried around the top corner to form a vertical density profile in the environment. The profile is stretched due to the different mass flux between different pairs of constant-density surfaces; but the main qualitative feature remains – that the magnitude of the density gradient decreases smoothly and monotonically away from the top surface (i.e. it increases with height and there is no first front).

The intermediate-time behaviour of neither system is easily accessible to analysis, though approximate expressions for the time-dependent profiles in a filling box with a turbulent plume were obtained by Worster & Huppert (1983). However, some insight can be obtained by considering the steady state which exists after a long time in the cases of a turbulent plume (Baines & Turner 1969) and of a laminar filling box with a constant flux applied to the sidewalls (Worster 1983). Both these studies show that if vertical diffusion is ignored in the steady state then

$$\psi_0(z) T'(z) = \text{constant}$$

in the environment. Differentiating this expression with respect to  $z$ , we obtain

$$\frac{T''}{T'} = -\frac{\psi_0'}{\psi_0}. \quad (26)$$

Since  $\psi_0$  is always positive (26) shows that the magnitude of the density gradient decreases with height if the boundary layer is entraining ( $\psi_0' > 0$ ) and increases with height if the boundary layer is detraining ( $\psi_0' < 0$ ). Although this result is calculated for a steady state it is likely to be approximately true in the time-dependent regime which may be treated as quasi-steady (e.g. Worster & Huppert 1983).

As we hinted in the introduction, this work was initially motivated by the authors' interest in the evolution of magma chambers. Through experiments and subsidiary analysis we have gained a thorough physical understanding of the fluid dynamics of filling boxes, and of the differences that arise when the convection is in the form of a laminar boundary layer rather than a turbulent plume. In addition we have developed a theoretical model which accurately predicts the stratification rate in a laminar filling box. The principles detailed in this paper should be applied when formulating geological models of magma evolution but we would advise caution before applying the present quantitative results directly. The geological problem is complicated by the strong dependence on temperature and composition of the fluid viscosity, and by the fact that thermal and compositional variations can have opposing effects on the density field and lead to a bi-directional boundary layer. These additional effects are the subject of current research.

We would like to thank our supervisors H. E. Huppert and J. S. Turner for their guidance, D. L. Corrigan and R. Wylde-Browne for technical assistance with the experiments, and many others at the R.S.E.S. for useful and stimulating discussions. The experiments were conducted while M.G.W. was visiting the R.S.E.S., a trip made possible by financial support from Trinity College and the D.A.M.T.P. Cambridge, and from the S.E.R.C.

## REFERENCES

- BAINES, W. D. & TURNER, J. S. 1969 Turbulent buoyant convection from a source in a confined region. *J. Fluid Mech.* **37**, 51–80.
- CHEN, C. F. & TURNER, J. S. 1980 Crystallization in a double-diffusive system. *J. Geophys. Res.* **85**, 2573–2593.
- ELDER, J. W. 1965 Turbulent free convection in a vertical slot. *J. Fluid Mech.* **23**, 99–111.
- GERMELES, A. E. 1975 Forced plumes and mixing of liquids in tanks. *J. Fluid Mech.* **71**, 601–623.
- GILL, A. E. 1966 The boundary-layer regime for convection in a rectangular cavity. *J. Fluid Mech.* **26**, 515–536.
- HIEBER, C. A. & GEBHART, B. 1971 Stability of vertical natural convection boundary layers: expansion at large Prandtl number. *J. Fluid Mech.* **49**, 577–591.
- HORNE, E. P. W. & TOOLE, J. M. 1980 Sensor response mismatches and lag correction techniques for temperature-salinity profilers. *J. Phys. Oceanogr.* **10**, 1122–1130.
- KILLWORTH, P. C. 1977 Mixing on the Weddell Sea continental slope. *Deep-Sea Res.* **36**, 427–448.
- KUIKEN, H. K. 1968 An asymptotic solution for large Prandtl number free convection. *J. Engng Maths* **2**, 355–371.
- LEITCH, A. M. 1985 Laboratory models of magma chambers. Ph.D. thesis, Australian National University, Canberra.
- MCBIRNEY, A. R. 1980 Mixing and unmixing of magmas. *J. Volcanol. Geotherm. Res.* **7**, 357–371.
- OSTRACH, S. 1964 Laminar flows with body forces. In *Theory of Laminar Flows* (ed. F. K. Moore). Princeton University Press.
- PATTERSON, J. & IMBERGER, J. 1980 Unsteady natural convection in a rectangular cavity. *J. Fluid Mech.* **100**, 65–86.
- SCHWIND, R. G. & VLIET, G. C. 1964 Observations and interpretations of natural convection and stratification in vessels. *Proc. Heat Trans. and Fluid Mech. Inst.* 51–68.
- SEGUR, J. B. 1953 Physical properties of glycerol and its solutions. In *Glycerol* (ed. C. S. Miner & N. N. Dalton). American Chemical Society Monograph Series.
- SPARKS, R. S. J., MEYER, P. & SIGURDSSON, H. 1980 Density variations amongst mid-ocean ridge basalts: implications for magma mixing and the scarcity of primitive lavas. *Earth Planet. Sci. Letter* **46**, 419–430.
- SPARROW, E. M. & GREG, J. L. 1956 Laminar free convection from a vertical plate with uniform surface heat flux. *Trans. A.S.M.E.*
- TURNER, J. S. 1979 *Buoyancy Effects in Fluids*. Cambridge University Press.
- WORSTER, M. G. 1983 Convective flow problems in geological fluid mechanics. Ph.D. thesis, University of Cambridge.
- WORSTER, M. G. & HUPPERT, H. E. 1983 Time-dependent density profiles in a filling box. *J. Fluid Mech.* **132**, 457–466.